Hermite Closures for Numerical Simulations of Kinetic Turbulence in Strongly Magnetized Plasmas

Maria Luísa da Silva Vilelas
Under supervision of Dr. Nuno Filipe Gomes Loureiro
Dep. Physics, IST, Lisbon, Portugal
November 2013

Abstract

Two closure conditions in order to truncate the set of coupled fluid-like equations originated by the expansion in Hermite polynomials of the "reduced" electron distribution function g_e of a reduced kinetic mode (*KREHM* [Zocco and Schekochihin, Phys. Plasmas **18**, 102309 (2011)]) valid for low-β, strongly magnetized plasmas are presented, where β is the ratio of the plasma pressure to the magnetic pressure and is ordered similiar to the electron-ion mass ratio, m_e/m_i. The two closure conditions for the Hermite hierarchy of equations were studied using two different dissipation operators: the Lénard-Bernstein collision operator and the hyper-collisions operator. Both closures, $g_{M+1} = 0$ and $g_{M+1} = (\rho_s/d_e)\sqrt{M+1}/(D_{M+1})\{A_\parallel, g_M\}$, present a similar behaviour for each one of the operators, where the second operator is the best to perform numerical simulations; with it we only needed to compute at least $M = 15$ to get an error inferior than 1%.

1 Introduction

Plasma is a ubiquitous form of matter in the Universe. It is nearly always found to be magnetized and turbulent. Very interesting examples include turbulence in the interstellar medium [1], which is stirred by violent events like supernovae explosions; turbulence in accretion flows around black holes [1]; turbulence in the solar wind streaming outward from the Sun [1]; and turbulence in nuclear fusion experiments in laboratories [2]. Put simply, we can say that we are dealing with a turbulent system if chaotic fluctuations of some field(s) over a broad range of scales are detected. In a plasma, these fluctuating fields are the electric and magnetic fields and the distribution functions of the particles. So, *turbulence is multiscale disorder* [3]. The comprehension of the dynamics of turbulent systems remains one of the greatest problems in theoretical physics.

When we are in the presence of a weakly collisional plasma, *i.e.*, when the collisional frequency is much lower than the characteristic frequencies of the turbulence, a plasma cannot be described as a conducting fluid (MHD theory) and a more general approach is required. This is provided by Kinetic Theory, namely, the 6D Vlasov equation for the particles distribution functions.

The kinetic representation of a plasma is naturally much more complex that the fluid representation. This means that, whilst at macroscopic scales the understanding of turbulence remains elusive, in weakly collisional plasmas, it is still very incipient. Given the analytical difficulties of the mathematical treatment of turbulence, one tool that is extremely useful to clarify the dynamics of turbulent plasmas is the direct numerical simulation.

In certain cases, it is possible to reduce the size and complexity of the problem and to find reduced kinetic models. One example is the gyrokinetic representation of strongly magnetized plasmas [4, 5, 6, 7]. Here, a reduced kinetic model (*Kinetic Reduced Electron Heating Model* [8]) will be used, which is valid for strongly magnetized plasmas with a low-β, where β is the ratio of the plasma pressure to the magnetic pressure, $\beta = 8\pi P/B^2$. For example, the solar corona is a plasma with these characteristics [9]. Using the low-β, where β is ordered similar to the electron to ion mass ratio m_e/m_i, as asymptotic expansion parameter allows the simplification of the six-dimensional kinetic theory to a four-dimensional reduced model (the three-dimensional configuration space plus the component parallel to the magnetic field of the velocity vector). This reduced kinetic model is naturally much simpler than the six-dimensional kinetic description, allowing computational studies that in the general case are prohibitive.

In this work, we explore a Hermite (spectral) representation of velocity-space. The Hermite transform of the electron distribution function converts the electron kinetic equation into a set of coupled, fluid like equations. The Hermite representation has the advantage of being simpler and more accurate, from the numerical point of view, besides making transparent certain kinetic processes such as the phase-mixing. However, the Hermite formulation introduces a difficulty: the equation for the mth Hermite moment depends on the $(m+1)$st moment, introducing a problem which concerns the closure (or truncation) of the equations.

Here we analyse two different closing schemes for the Hermite hierarchy of equations. Firstly, it is necessary to check if the chosen closure does not affect the linear physics of these equations, namely, if it captures the Landau damping in a correct way. An ideal closure should be able to capture the Landau damping rates with as few Hermite moments as possible. Finding a satisfying closure is a fundamental step in the applications of this physical model in the study of the turbulence in strongly magnetized plasmas.

This paper is organized as follows: in section 2 we intro-

duce the *Kinetic Reduced Electron Heating Model* [8] and in section 3 we present two different closure models investigated here. In section 4, the dynamics of the system using the different closures and different dissipation operators (Lénard-Bernstein and hyper-collisions) is studied and in section 5 some conclusions are presented.

2 Theoretical Formulation

We begin by introducing a fluid-kinetic approximation applicable to low-β plasmas, the *Kinetic Reduced Electron Heating Model (KREHM)*[8], where β, the ration of the plasma pressure to the magnetic pressure, is ordered similar to the electron-ion mass ratio m_e/m_i. We can define the perturbed electron distribution function to lowest order in $\sqrt{m_e/m_i} \sim \sqrt{\beta}$ and in the gyrokinetic expansion [4, 5] $\delta f_e = g_e + \left(\delta n_e/n_{0e} + 2v_\parallel u_{\parallel e}/v_{th_e}^2\right) F_{0e}$, where F_{0e} is the equilibrium Maxwellian, $v_{th_e} = \sqrt{2T_{0e}/m_e}$ is the electron thermal speed (with T_{0e} as the mean electron temperature), $v_\parallel$ is the parallel velocity coordinate, $\delta n_e/n_{0e}$ is the electron density perturbation (the zeroth moment of δf_e) normalized to its background value n_{0e}, and $u_{\parallel e} = e/(cm_e)d_e^2\nabla_\perp^2 A_\parallel$ is the parallel electron flow (the first moment of δf_e). $A_\parallel$ is the parallel component of the vector potential and $d_e = c/\omega_{p_e}$ is the electron skin depth. All moments of δf_e higher than δn_e and $u_{\parallel e}$ are contained in g_e, the "reduced" electron distribution function. The dynamics of the plasma is described by the evolution of $\delta n_e/n_0$, $A_\parallel$ and g_e and in the 2D case is [8]:

$$\frac{1}{n_0}\frac{d\delta n_e}{dt} = \frac{1}{B_z}\left\{A_\parallel, \frac{e}{cm_e}d_e^2\nabla_\perp^2 A_\parallel\right\}, \tag{1}$$

$$\frac{d}{dt}\left(A_\parallel - d_e^2\nabla_\perp^2 A_\parallel\right) = -\frac{cT_{0e}}{eB_z}\left\{A_\parallel, \frac{\delta n_e}{n_{0e}} + \frac{\delta T_{\parallel e}}{T_{0e}}\right\}, \tag{2}$$

$$\frac{dg_e}{dt} - \frac{v_\parallel}{B_z}\left\{A_\parallel, g_e - \frac{\delta T_{\parallel e}}{T_{0e}F_{0e}}\right\} = C[g_e] - \left(1 - \frac{2v_\parallel^2}{v_{th_e}^2}\right)\frac{F_{0e}}{B_z}\left\{A_\parallel, \frac{e}{cm_e}d_e^2\nabla_\perp^2 A_\parallel\right\}. \tag{3}$$

$C[g_e]$ is the collision operator, $\{P,Q\} = \partial_x P\partial_y Q - \partial_y P\partial_x Q$ is the Poisson bracket, $\nabla_\perp = \partial_x^2 + \partial_y^2$ and $d/dt = \partial/\partial t + c/B_z\{\varphi, \ldots\}$, B_z is the out-of-plane magnetic guide-field and φ is the electrostatic potential, wich is obtained from the gyrokinetic Poisson's law

$$\delta n_e/n_{0e} = 1/\tau\left(\hat{\Gamma}_0 - 1\right)e\varphi/T_{0e}, \tag{4}$$

where $\tau = T_{0i}/T_{0e}$ and $\hat{\Gamma}_0$ is an integral operator that expresses the average of electrostatic potential over rings of radius ρ_i. In Fourier space, this operator becomes $\Gamma_0(b) = \exp(-b)I_0(b)$, where $b = k_\perp^2\rho_i^2/2$ and I_0 is the modified Bessel function of the zeroth order [10] ($\rho_i = v_{th_i}/\Omega_i$ is the ion Larmor radius). Equations (1 - 3) constitute a minimal physically realizable paradigm for low-frequency nonlinear plasma dynamics with a strong guide field, including important effects such as ion Finite Larmor Radius, electron inertia, electron Landau damping and collisions.

The velocity-space dynamics and the emergence of small-scale structure in $v_\parallel$ are best understood in terms of the expansion of the electron distribution function g_e in Hermite polynomials [2, 11, 12, 13]. Noticing that equation (3) does not contain an explicit dependence on the perpendicular velocity coordinate $v_\perp$, we can consider that it has been integrated out, leaving us with $g_e = g_e(x, y, v_\parallel, t)$. We can now introduce the Hermite expansion,

$$g_e(x,y,t,v_\parallel) = \sum_{m=2}^{\infty} H_m\left(v_\parallel/v_{th_e}\right) g_m(x,y,t)F_{0e}(v_\parallel)/\sqrt{2^m m!}, \tag{5}$$

where the g_0 and g_1 coefficients do not show up in the sum because $g_0 = g_1 = 0$ due to the decomposition of δf_e adopted above. After some straightforward algebra, equation (3) becomes a series of coupled, fluid-like equations for each of the coefficients g_m:

$$\frac{dg_m}{dt} = \frac{v_{th_e}}{B_z}\left(\sqrt{\frac{m+1}{2}}\left\{A_\parallel, g_{m+1}\right\} + \sqrt{\frac{m}{2}}\left\{A_\parallel, g_{m-1}\right\}\right) + \frac{\sqrt{2}}{B_z}\delta_{m,2}\left\{A_\parallel, \frac{e}{cm_e}d_e^2\nabla_\perp^2 A_\parallel\right\} - D_m g_m, \tag{6}$$

where $\delta_{m,2}$ is a Kronecker delta and D_m is a dissipation operator (the Hermite transform of the collision operator). We will consider two forms for the dissipation operator. First, it will take the form of the Lénard-Bernstein collision operator, whose Hermite transform is

$$D_m = \nu_{ei} m, \tag{7}$$

with ν_{ei} the electron-ion collision frequency. However, due to its linear dependence on m, this operator forces us to solve a large number of Hermite polynomials in order to resolve the velocity-space cutoff as $\nu_{ei} \to 0$. Second, it will take the form of a hyper-collisions operator,

$$D_m = \nu_H\left(m/M\right)^\alpha, \tag{8}$$

where M is the highest Hermite moment. This operator introduces an artificial dissipation range in the system without introducing any non-physical effects (this is actually not obvious, as evidenced by figure 10). Although it is

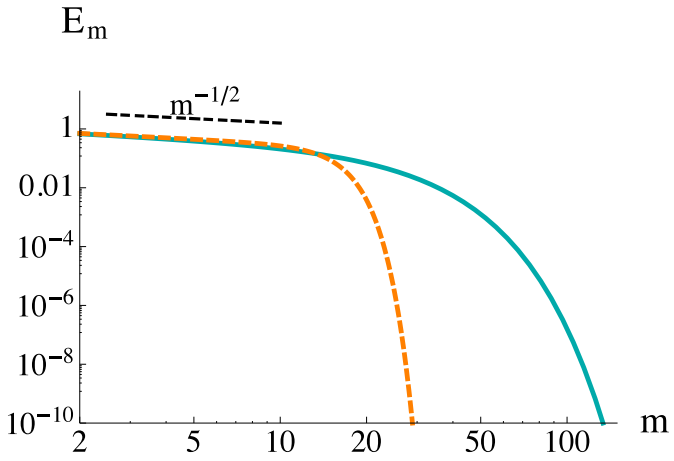

Figure 1: Graphical representation of the Hermite spectrum E_m as function of m. When $m \ll m_c$, the energy spectrum scales as $E_m \sim m^{-1/2}$. In blue we have the Hermite spectrum for the Lénard-Bernstein collision operator, where $\nu_{ei}\tau_A = 0.1$, and in orange, for the hyper-collisions operator, where $\nu_H\tau_A = 50$, $\alpha = 4$ and $M = 25$. The Hermite spectrum cutoff is given by $m_c = 17.8$ for the Lénard-Bernstein collision operator and $m_c = 14.6$ for the hyper-collisions operator.

used purely for numerical reasons, it is able to reproduce important physical effects, such as the Landau damping.

The Hermite formalism allows us to derive very concise derivations of important results [8], such as the Hermite spectrum. Linearizing equation (6) for a given k_y and defining the Hermite spectrum as $E_m = |g_m|^2/2$, we find that it evolves as

$$\frac{\partial E_m}{\partial t} = -|k_y|\frac{B_y}{B_z}v_{th_e}\frac{\partial}{\partial m}\sqrt{2m}E_m - 2D_m E_m. \quad (9)$$

In here, we will find a steady-state solution for equation (9) for both of the dissipation operators mentioned before. For the Lénard-Bernstein collision operator, given by equation (7), the solution for equation (9) is [8]

$$E_m = \frac{C(k_y)}{\sqrt{m}}\exp\left[-\left(\frac{m}{m_c}\right)^{3/2}\right], \quad (10)$$

where m_c stands for the collisional cutoff and is given by

$$m_c = \left(\frac{3}{2\sqrt{2}}\frac{B_y}{B_z}\frac{v_{th_e}|k_y|}{\nu_{ei}}\right)^{2/3}. \quad (11)$$

Concerning the hyper-collisions operator, which is given by equation (8), the solution for equation (9) is given by [14]

$$E_m = \frac{C(k_y)}{\sqrt{m}}\exp\left[-\left(\frac{m}{m_c}\right)^{(2\alpha+1)/2}\right]. \quad (12)$$

The collisional cutoff m_c is given by

$$m_c = \left(\frac{(1/2+\alpha)}{\sqrt{2}}\frac{B_y}{B_z}\frac{v_{th_e}|k_y|M^4}{\nu_H}\right)^{2/(2\alpha+1)}. \quad (13)$$

For both solutions, $C(k_y)$ is some function of k_y.

We can represent graphically the Hermite spectrum in steady-state for both collision operators. This result can be seen in figure 1.

We see that with the Lénard-Bernstein collision operator, the spectrum evolves smoothly with m (blue line) whilst for the hyper-collisions operator, we can see clearly the dissipation range (dashed orange line). We can also compute the values of m_c, given by equations (11) and (13). For the Lénard-Bernstein collision operator, with $\nu_{ei}\tau_A = 0.1$, we have $m_c = 17.8$ and for the hyper-collisions operator, with $\nu_H\tau_A = 50$, $\alpha = 4$ and $M = 25$, we have $m_c = 14.6$. With these values and the analysis of the behaviour of the dissipation range, we can predict how many Hermite moments we need to solve. Due to the smooth behaviour of the dissipation range for the Lénard-Bernstein collision operator, we need $M \gg 18$; concerning the hyper-collisions operator, the spectrum shows clearly the dissipation range, which means that we need $M > 15$.

3 Closures

Under proper normalization (for more detail see [14]), equations (1), (2) and (6) become

$$\frac{\partial n_e}{\partial t} + \{\varphi, n_e\} = \left\{A_\parallel, \nabla_\perp^2 A_\parallel\right\}, \quad (14)$$

$$\frac{\partial}{\partial t}\left(A_\parallel - d_e^2\nabla_\perp^2 A_\parallel\right) + \left\{\varphi, A_\parallel - d_e^2\nabla_\perp^2 A_\parallel\right\} = \eta\nabla_\perp^2 A_\parallel + \rho_s^2\left\{n_e + \sqrt{2}g_2, A_\parallel\right\}, \quad (15)$$

$$\frac{\partial g_2}{\partial t} + \{\varphi, g_2\} = \sqrt{3}\frac{\rho_s}{d_e}\left\{A_\parallel, g_3\right\} + \sqrt{2}\left\{A_\parallel, \nabla_\perp^2 A_\parallel\right\}, \quad (16)$$

$$\frac{\partial g_m}{\partial t} + \{\varphi, g_m\} = \sqrt{m+1}\frac{\rho_s}{d_e}\left\{A_\parallel, g_{m+1}\right\} + \sqrt{m}\frac{\rho_s}{d_e}\left\{A_\parallel, g_{m-1}\right\} - D_m g_m. \quad (17)$$

We are in the presence of a infinite set of fluid-like coupled equations which means that at some finite number M the system must be truncated. Closures are necessary in the study of physical systems with a large number of degrees of freedom and when it is only possible to compute a small number of moments. An ideal closure must capture all the

physics (*e.g.*, Landau-damping) of the problem with as few moments as possible.

A closure condition that is usually adopted [2, 11, 12] is

$$g_{m+1} = 0. \tag{18}$$

However, it results in large oscillations in the distribution function [11, 12] ; this problem can be solved by including a dissipative term, the D_m dissipation operator.

Notice that for any collision frequencies, there is allways a sufficiently large m such that $D_m/\omega \gg 1$ is true since both D_m operators scale positively with m. Taking this into account, some terms of equation (17) can be neglected, such as dg_m/dt and $\{A_\parallel, g_{m+1}\}$. The latter can be neglected due to the fact in the dissipation range of the energy cascade, we have $g_{m+1}/g_m \ll 1$. Setting $m = M + 1$, we find

$$g_{M+1} = \frac{\rho_s}{d_e}\frac{\sqrt{M+1}}{D_{M+1}}\{A_\parallel, g_M\}, \tag{19}$$

which is a nonlinear closure and that is only valid in the limit $D_m \gg \omega$. From the derivation of this closure, we have the certainty that with it the solution converges if enough moments are kept.

4 Linear Tests

We can now proceed with the linearization of equations (14 - 17). We have n_e as the perturbed electron density, φ is the electrostatic potential, and the in-plane magnetic field is given by $\mathbf{B}_\perp = -\hat{\mathbf{z}} \times \nabla_\perp A_\parallel$ and the dissipation is provided by the D_m operator. To linearize, we assume that all fields can be written as

$$\begin{aligned}\chi &= \chi_{eq} + \chi^1(x, y, t) \\ &= \chi_{eq} + \chi^1(x)\exp(ik_y y)\exp(-i\omega t)\end{aligned} \tag{20}$$

where χ^1 represents small perturbations to the equilibrium (for more details on the linearization read [15]). We consider an equilibrium described by $\mathbf{B}_{\perp,eq} = B_0\hat{\mathbf{y}}$, with B_0 a constant and $n_{e,eq} = \varphi_{eq} = g_{m,eq} = 0$. The linearization of equations (14 - 17) thus yields a system of algebraic equations which, in matrix form, can be represented as follows:

$$\mathbb{M}\left[\begin{array}{ccccccc} n_e & A_\parallel & g_2 & g_3 & \cdots & g_M \end{array}\right]^T = 0, \tag{21}$$

where $\mathbb{M}$ is a tridiagonal matrix given by the system of equations. Its entries are:

$$\mathbb{M}_{j,j+1} = \left(iB_0k_\perp^2 k_y, i\sqrt{2}\frac{\rho_s^2}{1+d_e^2k_\perp^2}, -i\sqrt{3}\frac{\rho_s}{d_e}k_yB_0, \cdots, -i\sqrt{M}\frac{\rho_s}{d_e}k_yB_0\right) \tag{22}$$

$$\mathbb{M}_{j,j} = (-i\omega, -i\omega, -i\omega, -i\omega + D_3, \cdots, -i\omega + D_M) \tag{23}$$

$$\mathbb{M}_{j+1,j} = \left(ik_yB_0\left(\frac{\rho_s^2}{1+d_e^2k_\perp^2} + \frac{\rho_i^2}{1+d_e^2k_\perp^2}\frac{1}{2\left(\Gamma_0(b)-1\right)}\right), i\sqrt{2}k_yB_0k_\perp^2, -i\sqrt{3}\frac{\rho_s}{d_e}k_yB_0, \cdots, -i\sqrt{M}\frac{\rho_s}{d_e}k_yB_0\right), \tag{24}$$

where $j = 1, \cdots, M+1$. In order to find the dispersion relation, we need to compute Det $\mathbb{M} = 0$ and solve it in order to find $\omega_N(k_\perp)$, where the subscript N stands for *Numerical*. Since we have a $(M+1)\times(M+1)$ matrix, the dispersion relation will have $(M+1)$ solutions. We are interested in the least damped solution because the least damped mode is the dominant mode as time goes to infinity. We will compare our numerical solutions with the collisionless dispersion relation, which is given by [8]

$$\left[\zeta^2 - \tau\frac{k_\perp^2 d_e^2/2}{1-\Gamma_0(k_\perp^2\rho_i^2/2)}\right][1+\zeta Z(\zeta)] = \frac{1}{2}k_\perp^2 d_e^2, \tag{25}$$

where $\zeta(x) = \omega/|k_\parallel(x)|v_{th_e}$, $Z(\zeta)$ is the plasma dispersion function and $Z'(\zeta) = -2[1+\zeta Z(\zeta)]$. Its graphical representation for $\rho_i = 1$ and $d_e = 0.2$ can be seen in figure 2. In figure 3, we have the graphical representation of the damping as function of the frequency for this equation at $k_\perp d_e = 2$.

The error introduced by each closure is quantified by

$$\varepsilon_\omega(\%) = \frac{|\omega_A - \omega_N|}{\omega_A} \times 100, \tag{26}$$

$$\varepsilon_\gamma(\%) = \left|\frac{\gamma_A - \gamma_N}{\gamma_A}\right| \times 100, \tag{27}$$

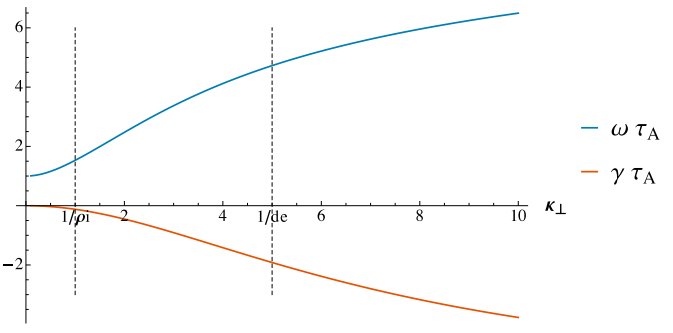

Figure 2: Graphical representation of the dispersion relation given by equation (25) for $\rho_i = 1$ and $d_e = 0.2$. The frequency is given by the blue line whislt the damping is given by the red one. Dashed lines identify the locations where $k_\perp\rho_i = 1$ and $k_\perp d_e = 1$.

where A stands for *Analytical* and it will be always computed at $k_\perp d_e = 2$ where d_e is the smallest physically meaningful spatial scale. We will declare a closure acceptable if, for $m = M$, it yields an error $\varepsilon_{\omega,\gamma} \lesssim 1\%$. Finally,

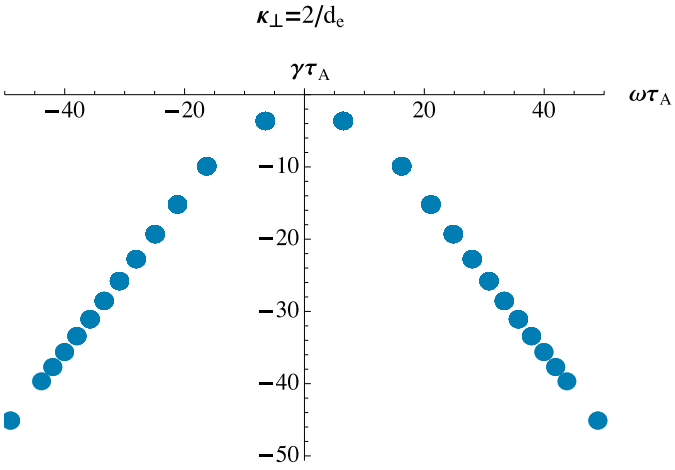

Figure 3: Graphical representation of the damping as function of the frequency for a chosen $k_\perp$ for equation (25).

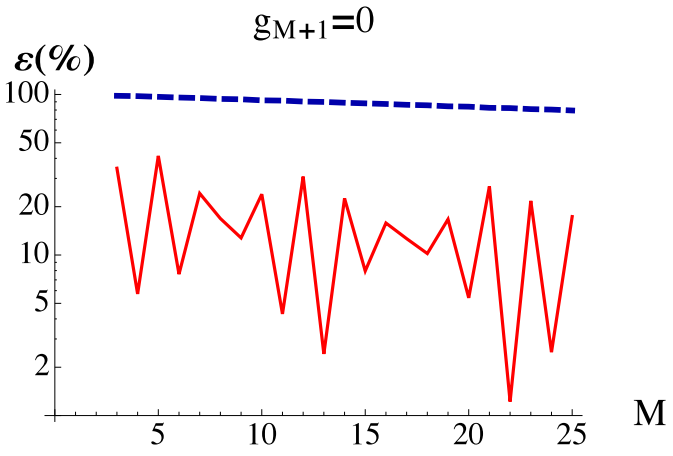

Figure 4: Error as function of M for the closure $g_{M+1} = 0$ with the Lénard-Bernstein collision operator, $D_m = m\nu_{ei}$. The red line stands for the error of the frequency ω and the blue, dashed line corresponds to the error of the damping γ. The error was computed at $k_\perp d_e = 2$. The convergence rate for the damping is $a^\gamma = 0.0096$.

we note that we expect the error to decrease exponentially with M, as is characteristic of spectral methods. All the computational results were obtained using the computational software program *Mathematica 9.0.0.0*.

4.1 The Lénard-Bernstein collision operator

First, we start by using the Lénard-Bernstein collision operator, $D_m = \nu_{ei} m$. We begin to plot the error as function of M for both of the closures: $g_{m+1} = 0$ which is the simplest and usually adopted one, and $g_{M+1} = (\rho_s/d_e)\sqrt{M+1}/(D_{M+1})\{A_\parallel, g_M\}$, which is guaranteed to converge as $M \to \infty$. Due to its linear dependence on m, with this operator we need to compute a large number of moments, however, due to computational limitations, the tests were performed up to $M = 25$ (*Mathematica* has trouble solving equation (21) for larger values of M). We chose $\nu_{ei}\tau_A = 0.1$ for the electron-ion collision frequency. For comparison, we note that in the solar wind [16] we have $\nu_{ei}\tau_A = 4.2\times10^{-6}$, a much smaller value which, however, would require an unfeasibly large number of Hermite moments in order to solve the velocity space dynamics.

In figure 4 we have the error for the closure $g_{M+1} = 0$ and in figure 5, we have the error for the closure $g_{M+1} = (\rho_s/d_e)\sqrt{M+1}/(D_{M+1})\{A_\parallel, g_M\}$, both as function of M.

We see that the error of the damping converges exponentially, as expected, but the same does not happen with the error of the frequency, which presents a very oscillatory behaviour. Recalling the Hermite spectrum in figure 1, we saw that we needed $M \gg 18$. Since we are limited until $M = 25$, we can conclude that the number of moments we are solving is not large enough to capture the convergence of the error, resulting in these large oscillations. Besides that, these oscillations are due to the jumping from one solution to the next one and due to the fact that the system may be sensitive to even and odd values of M.

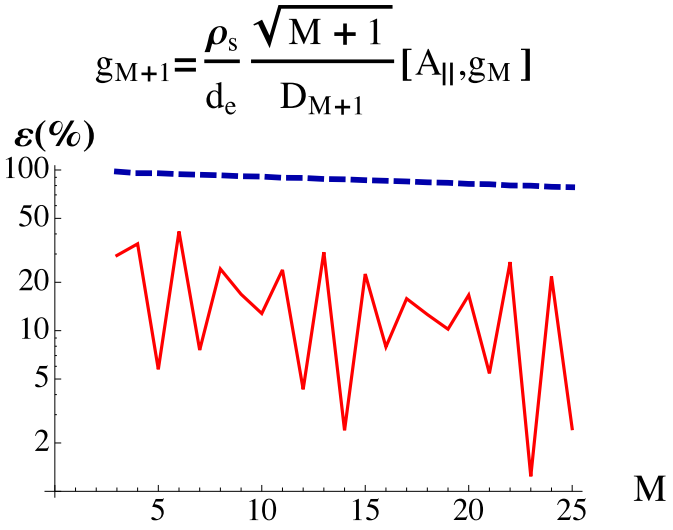

Figure 5: Error as function of M for the closure $g_{M+1} = (\rho_s/d_e)\sqrt{M+1}/(D_{M+1})\{A_\parallel, g_M\}$ with the Lénard-Bernstein collision operator, $D_m = m\nu_{ei}$. The red line stands for the error of the frequency ω and the blue, dashed line corresponds to the error of the damping γ. The error was computed at $k_\perp d_e = 2$. The convergence rate for the damping is $a^\gamma = 0.0099$.

4.2 The hyper-collisions operator

Here we will use the hyper-collisions operator, $D_m = \nu_H (m/M)^\alpha$. We want some values of α and ν_H such that we have weak or no damping at low m, to garantee the existence of an inertial range. This can be translated as

$$\frac{\nu_H (m/M)^\alpha}{\omega} \ll 1, \quad m \ll M, \tag{28}$$

$$\frac{\nu_H (m/M)^\alpha}{\omega} \gg 1, \quad m \sim M. \tag{29}$$

Concerning the value for α, making $\alpha \gg 1$ would progressively concentrate the damping in fewer and fewer modes (at higher m) but it cannot be very large because of the possibility of bottleneck effects [23]. For that reason we choose $\alpha = 4$. Relatively to the value of ν_H, analysing figure 2, we see that we have $\omega^{Max}\tau_A \sim 6.5$. Choosing $m = M/2$ and $m = M$ and replacing it in equations (28) and (29), respectively, we get $\nu_H (1/2)^4 / \omega^{Max} \ll 1$ and $\nu_H/\omega^{Max} \gg 1$, which leads to $\omega^{Max} \ll \nu_H \ll 2^\alpha \omega^{Max}$. Notice that α is the parameter that changes the range from which we can choose the value for ν_H: this range increases with α. We will choose $\nu_H = 50$.

The graphical representation of the error as function of M for both closures can be seen in figures 6 and 7.

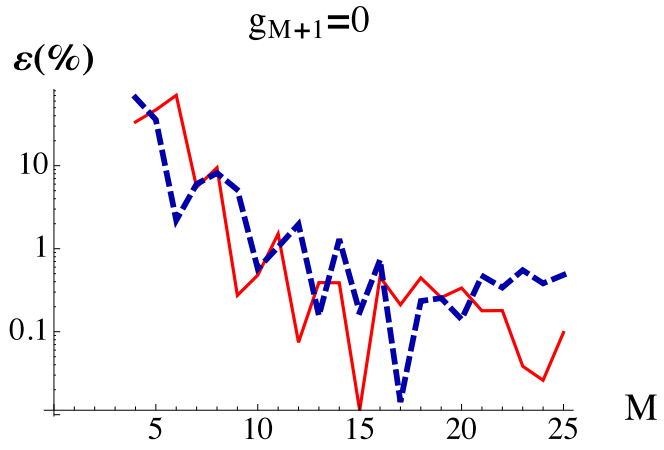

Figure 6: Error as function of M for the closure $g_{M+1} = 0$ at $k_\perp d_e = 2$. The red line stands for the error of the frequency ω and the dashed blue line corresponds to the error of the damping γ. The condition $\varepsilon_{\omega,\gamma} \lesssim 1\%$ is valid for $M \geq 15$. The convergence rate for the frequency is $a^\omega = 0.31$ and $a^\gamma = 0.19$ for the damping.

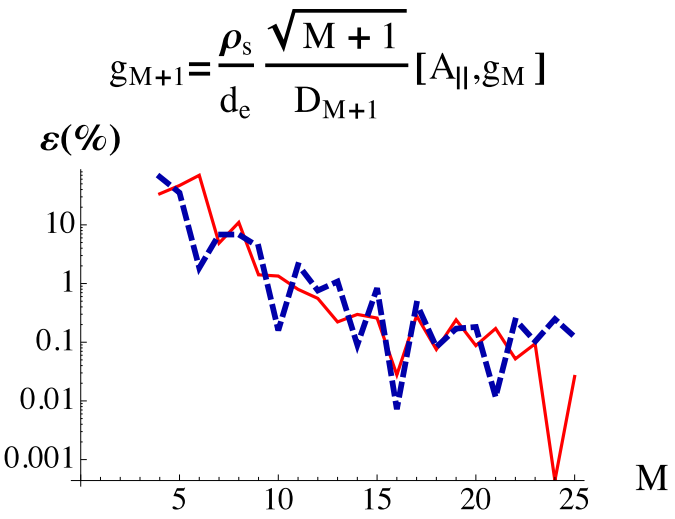

Figure 7: Error as function of M for the closure $g_{M+1} = (\rho_s/d_e)\sqrt{M+1}/(D_{M+1})\{A_\parallel, g_M\}$ at $k_\perp d_e = 2$. The red line stands for the error of the frequency ω and the blue, dashed line corresponds to the error of the damping γ. An error that satisfies $\varepsilon_{\omega,\gamma} \lesssim 1\%$ is given for $M \geq 14$. The convergence rate for the frequency is $a^\omega = 0.30$ and $a^\gamma = 0.20$ for the damping.

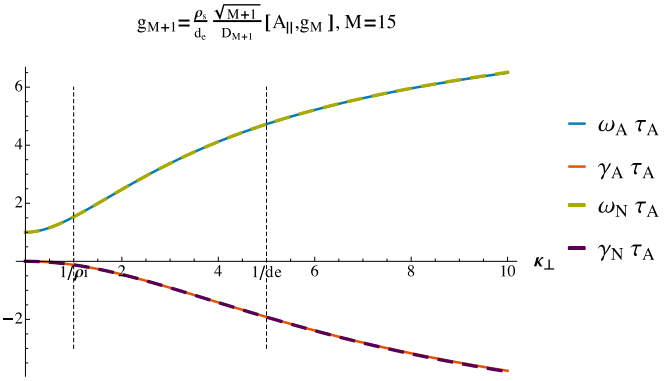

Figure 8: Graphical representation of the dispersion relation for the closure $g_{M+1} = (\rho_s/d_e)\sqrt{M+1}/(D_{M+1})\{A_\parallel, g_M\}$ and $M = 15$. The error for the frequency is $\varepsilon_\omega = 0.15\%$ and the error for the damping is $\varepsilon_\gamma = 0.45\%$, for $k_\perp d_e = 2$.

For both closures, there exists an oscillatory behaviour for both the error of the frequency and of the damping. One justification for these oscillations is the fact that the system is sensitive to even and odd values of M. Another justification for the oscillations is due to the jumping from one solution to the next one. The error decreases exponentially, as expected, since this is one property of the spectral methods. We also get an error $\varepsilon_{\omega,\gamma} \lesssim 1\%$ for both closures: for the $g_{M+1} = 0$ closure, we only need to compute at least $M = 15$; for the nonlinear closure, we only need at least $M = 14$. Both these values agree with the collisional cutoff that was found previously. The dispersion relation for the nonlinear closure with $M = 15$ is represented in figure 8.

The graphical representation of the damping as function of the frequency for both closures and both collision operators at $k_\perp d_e = 2$ and for $M = 15$ can be seen in figures 9 and 10.

The spectrum shows a very different behaviour for both collision operators. With the Lénard-Bernstein collision operator, the least damped modes are very distant from the least damped mode of the analytical solution, confirming that a larger M is required. Concerning the hyper-collisions operator, all the least damped modes coincide, as expected. However, with this collision operator, the spectrum shows a very distinct behaviour from the analytical solution and the possibility of non-physical behaviour in nonlinear simulations (where modes other than the least damped ones may be important) cannot be ruled out and warrants future investigation.

5 Conclusions

In this work, two closure conditions were studied in order to truncate a set of coupled fluid-like equations originated by the expansion in Hermite polynomials of the electron distribution function g_e of a kinetic reduced model,

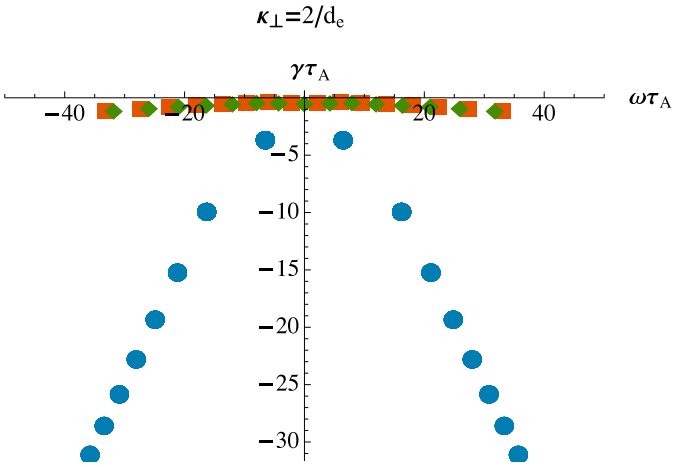

Figure 9: Graphical representation of the damping as function of the frequency for $g_{M+1} = 0$ and $g_{M+1} = (\rho_s/d_e)\sqrt{M+1}/(D_{M+1})\{A_\parallel, g_M\}$ at $k_\perp = 2/d_e$ for the Lénard-Bernstein collision operator for $M = 15$. In the blue dots we have the analytical solution, which can also be seen in figure 3, in orange we have the solutions for the closure $g_{M+1} = 0$ and in the green, the solutions for the closure $g_{M+1} = (\rho_s/d_e)\sqrt{M+1}/(D_{M+1})\{A_\parallel, g_M\}$.

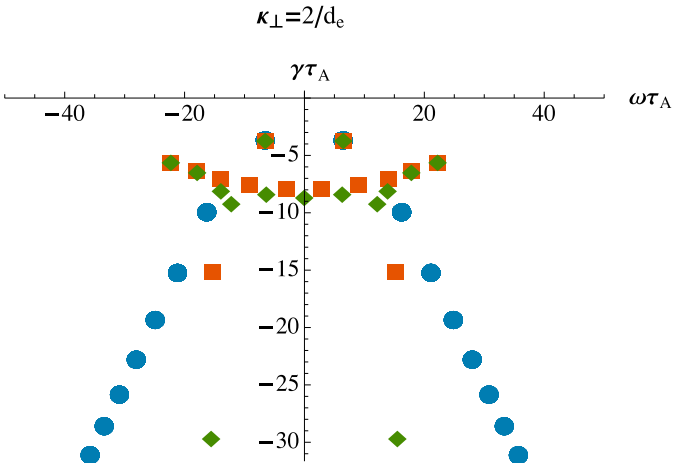

Figure 10: Graphical representation of the damping as function of the frequency for $g_{M+1} = 0$ and $g_{M+1} = (\rho_s/d_e)\sqrt{M+1}/(D_{M+1})\{A_\parallel, g_M\}$ at $k_\perp = 2/d_e$ for the hyper-collisions operator, for $M = 15$. In the blue dots we have the analytical solution, which can also be seen in figure 3, in orange we have the solutions for the closure $g_{M+1} = 0$ and in the green, the solutions for the closure $g_{M+1} = (\rho_s/d_e)\sqrt{M+1}/(D_{M+1})\{A_\parallel, g_M\}$.

KREHM [8]. The simulations for both closures, $g_{m+1} = 0$ and $g_{M+1} = (\rho_s/d_e)\sqrt{M+1}/(D_{M+1})\{A_\parallel, g_M\}$, were performed using two dissipation operators, the Lénard-Bernstein collision operator and the hyper-collisions operator. Although the behaviour of the system for both closures is similar, it changes with the dissipation operator. With the Lénard-Bernstein collision operator, a large number of Hermite moments has to be solved in order to get an error for the frequency and the damping of the dispersion relation of 1%; with the hyper-collisions operator, we only need $M = 15$. These values were confirmed with the Hermite spectrum cutoff, m_c.

References

[1] A. A. Schekochihin and S. C. Cowley (2007). *Magnetohydrodynamics — Historical Evolution and Trends*, Springer.

[2] G. W. Hammett, M. A. Beer, W. Dorland, S. C. Cowley and S. A. Smith (1993). *Developments in the Gyrofluid Approach to Tokamak Turbulence Simulations*, Plasma Physics and Controlled Fusion, **35**, 973.

[3] A. A. Schekochihin, S. C. Cowley, W. Dorland, G. W. Hammett, G. G. Howes, G. G. Plunk, E. Quataert and T. Tatsuno (2008). *Gyrokinetic Turbulence: a nonlinear route to dissipation through phase space*, Plasma Physics and Controlled Fusion, **50**, 124024.

[4] E. A. Frieman and L. Chen (1982). *Nonlinear gyrokinetic equations for low-frequency electromagnetic waves in general plasma equilibria*, Physics of Fluids, **25**, 502.

[5] G. G. Howes, S. C. Cowley, W. Dorland, G. W. Hammett, E. Quataert and A. A. Schekochihin (2006). *Astrophysical Gyrokinetics: basic equations and linear theory*, The Astrophysical Journal, **651**, 590.

[6] A. J. Brizard and T. S. Hahm (2007). *Foundations of Nonlinear Gyrokinetic Theory*, Reviews of Modern Physics, **79**, 421.

[7] A. A. Schekochihin, S. C. Cowley, W. Dorland, G. W. Hammett, G. G. Howes, E. Quataert and T. Tatsuno (2009). *Astrophysical Gyrokinetics: kinetic and fluid turbulent cascades in magnetized weakly collisional plasmas*, The Astrophysical Journal Supplement Series, **182**, 310.

[8] A. Zocco and A. A. Schekochihin (2011). *Reduced fluid-kinetic equations for low-frequency dynamics, magnetic reconnection and electron heating in low-beta plasmas*, Physics of Plasmas **18**, 102309.

[9] D. A. Uzdensky (2007). *The Fast Collisionless Reconnection Condition and the Self-Organization of Solar Coronal Heating*, The Astrophysical Journal, **671**, 2139.

[10] M. Abramowitz and I. A. Stegun (1972). *Handbook of Mathematical Functions with Formulas, Graphs and Mathematical Tables*, National Bureau of Standards Applied Mathematics Series.

[11] L. Gibelli and B. D. Shizgal (2006). *Spectral convergence of the Hermite basis function solution of the Vlasov equation: The free-streaming term*, Journal of Computational Physics, **219**, 477.

[12] F. C. Grant and M. R. Feix (1967). *Fourier-Hermite Solutions of the Vlasov Equations in the Linearized Limit*, The Physics of Fluids, **10**, 696.

[13] F. C. Grant and M. R. Feix (1967). *Transition between Landau and Van Kampen Treatments of the Vlasov Equation*, The Physics of Fluids, **10**, 1356.

[14] N. F. Loureiro, A. A. Schekochihin and A. Zocco (2013). *Fast collisionless reconnection and electron heating in strongly magnetized plasmas*, Physical Review Letters, **111**, 025002.

[15] N. F. Loureiro and G. W. Hammett (2008). *An iterative semi-implicit scheme with robust damping*, Journal of Computational Physics, **227**, 4518.

[16] R. M. Kulsrud (2005). *Plasma Physics for Astrophysics*, Princeton University Press.

[17] D. R. Nicholson (1983). *Introduction to Plasma Theory*, John Wiley & Sons, Inc.

[18] C. S. Ng, A. Bhattacharjee and F. Skiff (1999). *Kinetic Eigenmodes and Discrete Spectrum of Plasma Oscillations in a Weakly Collisional Plasma*, Physical Review Letters, **83**, 1974.

[19] V. Bratanov, F. Jenko, D. Hatch and S. Brunner (2013). *Aspects of linear Landau damping in discretized systems*, Physics of Plasmas, **20**, 022108.

[20] S. A. Smith and G. W. Hammett (1997). *Eddy viscosity and hyperviscosity in spectral simulations of 2D drift wave turbulence*, Physics of Plasmas, **4**, 978.

[21] G. Joyce, G. Knorr and H. K. Meier (1971). *Numerical Integration Methods of the Vlasov Equation*, Journal of Computational Physics, **8**, 53.

[22] G. Knorr and M. Shoucri (1974). *Plasma Simulation as Eigenvalue Problem*, Journal of Computational Physics, **14**, 1.

[23] M. K. Verma and D. Donzis (2007). *Energy transfer and bottleneck effect in turbulence*, Journal of Physics A: Mathematical and Theoretical, **40**, 4401.